**P4.27  SHORT WAVE AEROSOL DIRECT FORCING OVER CLOUD FREE OCEANS FROM TERRA**

Jianglong Zhang* and Sundar A. Christopher
University of Alabama in Huntsville, Huntsville, Alabama

**Abstract**

Satellite measurements from Terra are used to examine shortwave aerosol radiative forcing (SWARF) over cloud free oceans. Broadband measurements from the Clouds and Earth's Radiant Energy System (CERES) instruments are used to study the short wave aerosol effect (SWARF). The Moderate-Resolution Imaging Spectroradiometer (MODIS) aerosol and cloud products are used to discriminate aerosol scenes from totally clear and cloudy scenes of CERES pixels.   This study shows that for September 2000, the averaged aerosol optical thickness and SWARF are 0.07 and -6Wm$^{-2}$ respectively for CERES cloud free regions over global oceans.   Dust aerosols from the West Coast of Africa have higher SWARF values when compared with aerosols from biomass burning regions.

Preliminary results in cloudy conditions show that for observed cloud fraction values less than 20% within a CERES footprint, aerosol direct and indirect effects are dependent upon aerosol optical thickness (AOT) ranges. While aerosol indirect effect dominates at the low aerosol loading scenes, the aerosol direct effect dominates at the high aerosol loading scenes. Major sources of uncertainties in this study, such as cloud contamination and Angular Distribution Models (ADMs), must be carefully examined in future studies.

**1.      Introduction**

The understanding of aerosols and their radiative effects is important in climate forcing studies. Aerosols could directly reflect or absorb the incoming solar energy, thereby, altering the radiation balance of the earth atmosphere system [Kaufman et al., 2002].   Aerosols could also indirectly alter the climate system by modifying cloud properties, suppressing precipitation and evaporating low clouds [e.g. Ramanathan et. al, 2001].  The recent IPCC report notes that the

understanding levels of all aerosol types are either low or very low [IPCC, 2001].  Traditional ways of addressing aerosol climate effects, use either radiative transfer models or general circulation models (GCMs) [e.g. Hansen et al., 1998; Penner et al., 1992].   Characterizing the spatial and temporal distribution of aerosol physical and optical properties in models, remains a challenging problem. This is due to the short life span of the major types of aerosols, and the changing of aerosol properties as they interact with other atmospheric entities (such as other type of aerosols, gases, water vapor, and clouds) [e.g. Ramanathan et. al, 2001].

Recently, several studies have shown the potential of using satellite-retrieved top-of-the-atmosphere (TOA) fluxes to understand the radiative effect of aerosols.  Haywood et al., [1999] compared TOA shortwave (SW) fluxes derived from the Earth Radiation Budget Experiment (ERBE) and a GCM model to study the radiative effect of aerosols.   Christopher et al., [2000] studied the radiative effect of biomass burning over Central America by using collocated Clouds and Earth's Radiant Energy System (CERES) and Visible Infrared Scanner (VIRS) measurements from the Tropical Rainfall Measuring Mission (TRMM) platform.  Loeb and Kato (2002) have extended this approach to study the direct radiative forcing of aerosols over the oceans. This approach of using combined satellite measurements provides an independent method for studying the impact of aerosols on climate. NASA's suite of well-calibrated sensors on the Terra satellite provides an unprecedented opportunity to study the effect of aerosols on climate.   In this paper, we estimate the Short-Wave (SW) Aerosol Direct Forcing (SWARF) in cloud free regions over the global oceans using a combination of broadband data sets derived from CERES observations and data sets generated from Moderate-Resolution Imaging Spectro-radiometer (MODIS) measurements.

**2.      Data and Methodology**

The CERES ES-8 (ERBE like TOA instantaneous) data contains broadband TOA SW (0.3-5 $\mu$m) and longwave (5.0-50.0 $\mu$m) radiances and fluxes.   The fluxes are converted from radiances using Angular Dependence Models

*Corresponding Author address: Jianglong Zhang, Department of Atmospheric Sciences, University of Alabama-Huntsville, Huntsville, AL 35806; zhang@nsstc.uah.edu.

(ADM's) that relate observed radiances, at narrow solid angles, to the total fluxes comes from the reflecting surface using the empirical relations derived from ERBE [Wielicki et al., 1996]. The spatial resolution of the pixel-level CERES ES-8 data is roughly 30km at nadir. Currently these ADM's do not include aerosol types. Zhang and Christopher [2003, this issue] examine the effect of aerosol ADMs on the retrieved fluxes.

The MODIS aerosol product (MOD04) contains spectral aerosol optical thickness, the effective radius of the aerosol and the fraction of the total optical thickness contributed by the sub-micron size mode aerosol and other secondary parameters [Tanré et al., 1997]. Based on theoretical sensitivity studies, the uncertainties in AOT (at 0.55 μm) retrievals are estimated to be ± 0.05 ±0.05 AOT over oceans [Tanré et al., 1997]. The MODIS AOT product has been validated against sunphotometer derived values over oceans and recent results have showed that the MODIS algorithm is performing within the expected accuracy [Remer et al., 2002a].

The MOD06 product provides cloud top parameters, such as cloud top pressure and cloud top temperature, at 5 km resolution and cloud optical parameters, such as cloud optical thickness and cloud effective radius, at 1 km resolution [Platnick et al., 2002]. The MOD06 data also provides cloud fraction at 5 km resolution and cloud/no cloud information at both 1 and 5 km resolution. In this study, we take each CERES footprint and collocate the 5km- MOD06 data to identify cloud-free regions. For these cloud free regions, we obtain aerosol properties from the MOD04 data. Twenty-nine days of global CERES and MODIS (MOD04 and MOD06) data in September 2000 were used in this study (CERES ES-8 data from September 17th was unavailable) and is roughly equivalent to about 500GB of data.

The CERES pixels that are labeled as "clear ocean" by the CERES ES-8 data [Wielicki and Green, 1989] were first selected. However, due to the large footprint of the CERES scanner, these pixels could still have cloud contamination [Wielicki and Green, 1989]. To eliminate these cloud effects, the MOD06 data with a higher spatial resolution is collocated with the CERES data and only those CERES pixels with a 0% cloud fraction as identified by the MOD06 data were used. The CERES is collocated with MODIS data using a Point-Spread-Function (PSF) energy cutoff value of 96%. The MODIS pixels inside a CERES pixels are arithmetically averaged to obtain cloud fraction and aerosol information of the

CERES pixels. Our purpose is to exclude all cloudy CERES "clear ocean" pixels, and a stringent test used to exclude clouds within the CERES pixels.

The SWARF[*] at the top of the atmosphere (TOA) is defined as the difference between clear ($F_{clr}$) and aerosol ($F_{aer}$) fluxes [Christopher et al., 1996; 2001]. In this study, $F_{clr}$ and $F_{aer}$ were averaged over $2° \times 2°$ (latitude×longitude) bins. The $F_{aer}$ values are obtained by averaging the cloud free CERES ES-8 data within a $2° \times 2°$ bin. However, $F_{clr}$ is more difficult to obtain because when aerosol loading is low, satellite imagers are not effective in detecting aerosols [Remer et al., 2002b]. Tanré et al., [1997] estimated that the uncertainties in MOD04 AOT product to be ± 0.05 ± 0.05τ over ocean. In this study, an average increase in SW flux of ~5Wm$^{-2}$ is found when MODIS AOT changes from values near zero to values near 0.05, which implies that on the average, the uncertainties in MODIS AOT retrievals over ocean could be lower than what is estimated by Tanré et al., [1997]. King et al., [1999] showed that the uncertainties in MODIS AOT retrievals over ocean is 0.01± 0.05τ for selected cases during TARFOX. We therefore assume that all cloud free CERES pixels that have AOT < 0.02, as determined by the MODIS data, are aerosol free pixels and are used to obtain $F_{clr}$ values. However, the uncertainties in $F_{clr}$ induced by the uncertainties in MODIS AOT retrievals must be carefully examined. Our first order estimation shows that the uncertainties in $F_{clr}$ due to this assumption is on the order of 1Wm$^{-2}$.

## 3.  Results

Figure 1 shows the relationship between MODIS-retrieved AOT versus the CERES-derived SWARF. Each symbol in the figure represents the averaged AOT and SWARF values in a $2° \times 2°$ latitude-longitude bin. The SWARF is most sensitive to AOT changes when AOT is low and less sensitive to AOT changes when the aerosol loading is high. For example, a change in AOT from 0 to 0.05 causes a change in SWARF of -5.1 Wm$^{-2}$ and a change in AOT from 0.45 to 0.5 causes a change in SWARF of -2.3 Wm$^{-2}$. A second order polynomial fit through the data points yields the following relationship: SWARF = 0.35 - 105.34$\tau_{0.55}$ +61.47$\tau_{0.55}^2$ ($0 \leq \tau_{0.55} \leq 0.7$). The averaged AOT and SWARF is 0.07 and -6 Wm$^{-2}$ respectively for all the CERES cloud free areas

---

[*] SWARF = $F_{clr}$ - $F_{aero}$. Where $F_{aero}$ is the spatially averaged SW fluxes at the TOA in aerosol contaminated (cloud free) region, and $F_{clr}$ is the spatially averaged SW fluxes at the TOA when aerosols are absent.

over global ocean for September 2000. Also shown in the inset are the SW fluxes vs. AOT for
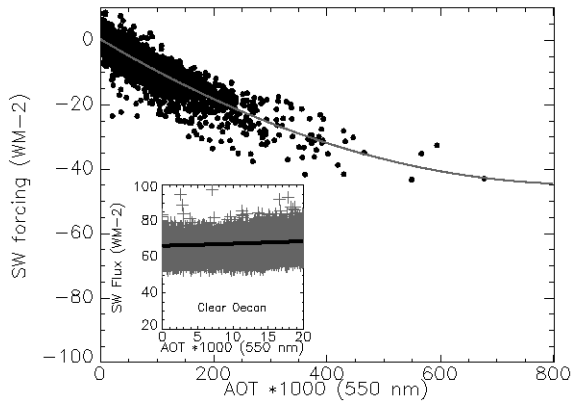


Figure 1. Averaged MODIS AOT*1000 (at 0.55μm) vs. SWARF. The solid black line shows a second-order polynomial fit. Inset shows the MODIS AOT*1000 (at 0.55μm) vs. CERES TOA SW fluxes for cloud free CERES pixels that have AOT less than 0.02. Only non-sunglint pixels are included in the analysis.

all the cloud free pixels that have AOT less than 0.02 (which are assumed to be cloud and aerosol free pixels in this study). The variations in SW fluxes in those cloud free, low aerosol loading pixels are due to three main reasons: the uncertainties in the clear sky ADM [Wielicki and Green, 1989], the solar zenith angle effect [Loeb and Kato, 2002], and the surface wind influence [Zhang and Christopher, this issue]. On the average, this is a ~2Wm$^{-2}$ increase in SW flux as AOT values change from 0 to 0.02. This induces an uncertainty in the derived SWARF on the order of 1Wm$^{-2}$. On the average, the TOA SW flux over ocean is 67.58±3 Wm$^{-2}$ in the study period.

We further studied the aerosol SW radiative forcing for several selected regions. The six areas are as follows; (1) South Africa (SA) (0-40°S, 30-50°E), (2) Australia (AUS) (0-20°S, 110-130°E), (3) East Asia (EA) (20-40°N, 110-130°E), (4) North Africa (NAF) (10-30°N, 10-40°W), (5) North America (NAM) (20-40°N, 60-80°W), and (6) Remote Ocean (RO) (20-40°S, 100-120°W). Figure 2 shows AOT versus the cloud-free SW flux for the six selected regions. A solid black line indicates the globally averaged value. When the AOT value is less than 0.2, all the selected regions, except NAF, share a similar SWARF pattern. This indicates that when the aerosol loading is low, the background aerosols are major contributors to SWARF. The NAF region,

dominated by dust aerosols, is most efficient in reflecting incoming solar energy when compared with other regions. The aerosols from the SA and AUS source regions have lower SWARF values when AOT is greater than 0.2. The slopes of AOT vs. SW flux for the SA and AUS regions are very similar, which implies that the aerosols in these two regions have similar radiative properties where the dominant aerosol type is from biomass burning [Husar et al., 1997; Olson et al., 1999]. Recent studies show that the single scattering albedo ($\omega_o$) of dust and smoke aerosols at 0.64 μm is 0.97 [Kaufman et al., 2001] and 0.86 [Reid et al., 1998] respectively. The higher $\omega_o$ values of dust leads to higher TOA SW values when compared with SW flux values for regions dominated by biomass burning and pollutant aerosols. One other reason for the higher TOA SW values over these regions is due to the different particle sizes of dust aerosols when compared to smoke aerosols. The biomass burning aerosols have smaller effective radius on the order of 0.15 μm [Reid et al., 1998] when compared to dust aerosols. The slope of AOT vs. SW flux for the EA region is between that of dust and smoke regions. The dominant aerosol type is from industrial pollution with different aerosol radiative characteristics when compared with dust
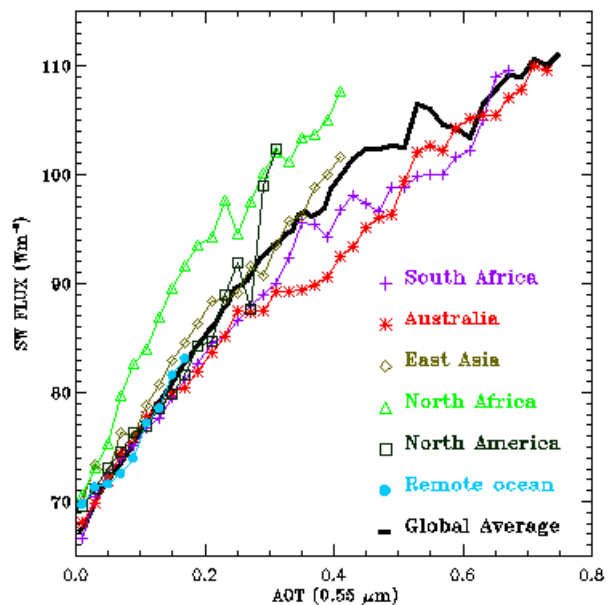


Figure 2. Averaged AOT (0.55μm) vs. CERES fluxes for six selected regions. Solid black line shows the globally averaged values.
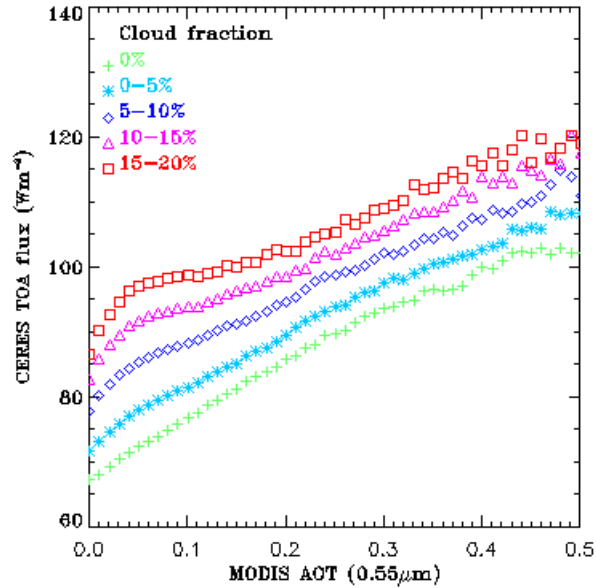
and smoke aerosols.  The slope of AOT vs. SW



Figure 3. MODIS AOT (0.55μm) vs. CERES fluxes for five different cloudiness range: 0%, 0-5%, 5-10%, 10-15%, and 15-20%.

flux for NAM is similar to regions dominated by smoke and pollutant aerosols such as SA and AUS when aerosol loading is low, and is similar to regions dominated by dust aerosols (NAF) when aerosol loading is high.

As shown in figure 1, the AOT and SW forcing have a non-linear relationship.  The non-linear relation is due to several reasons.  When the aerosol layer is optically thin, the reflected energy at the TOA is very sensitive to changes in AOT.  However, as the aerosol layer becomes thick, the reflected energy at the TOA becomes insensitive to the change in AOT and this is a function of aerosol types, surface types, and solar zenith angle [Ross et al., 1998].  Secondly, as shown in Figure 2, different aerosol types have

As mentioned in the previous section, the CERES "clear ocean" pixels contain low cloud contamination [Wielicki and Green, 1989].  In this study, we have examined the cloud fraction of each CERES pixel using collocated MODIS data. Since the CERES PSF of 96% cutoff is used, and the arithmetic average instead of the weight average of the MODIS cloud product is applied in computing the cloudiness, we overestimated the cloud fraction of a CERES pixel. However, it is interesting to examine the relationship between the cloud amount reported in this study and the aerosol forcing for the CERES "clear ocean " pixels.  Figure 3 shows the MODIS AOT versus the averaged CERES TOA SW fluxes for five different ranges of cloudiness: 0%, 0-5%, 5-10%, 10-15%, and 15-20%. The CERES "clear ocean" pixels from September 2000 are used, and each symbol represents the averaged CERES TOA SW fluxes within a 0.01 MODIS AOT bin.  A total of 1.45 million pixels are used in the analysis, and pixels that are within cloud fraction range of 0%, 0-5%, 5-10%, 10-15%, and 15-20% account for 27%, 41%, 19%, 13%, and 1% of the total number of collocated clear ocean pixels respectively. Since we include both clouds and aerosols in the study, the combined effects of the aerosol direct (reflect solar energy) and indirect forcing (due to aerosols modifying cloud properties) for low cloud fraction cases can be evaluated. As shown in figure 3, for AOT ranging from 0.05 to 0.5, the slope of AOT vs. flux decreases with an increase in cloud fraction whereas at the AOT range of 0 to 0.05, the slope of AOT vs. flux increases with increasing cloud fraction.  The absolute changes of CERES SW fluxes are 29.8, 30.2, 25.7, 25.7 and 21.9 Wm$^{-2}$ at the AOT range of 0.05 to 0.5, and are 5.1, 6.4, 7.5, 9.2 and 10.5 Wm$^{-2}$ at the AOT range of 0 to 0.05, for cloud fraction of 0%, 0-5%, 5-10%, 10-15% and 15-20% respectively. This preliminary analysis shows that the aerosol direct and indirect effects dominate at the different aerosol optical thickness regimes and is expressed as equation 1:

$$\frac{\partial(TOA\ SW\ flux)}{\partial(AOT)} = (1-c)*(aerosol\ direct\ effect)+c*(aerosol\ indirect\ effect) \qquad (1)$$

different aerosol forcing characteristics.  Dust aerosols are very effective in reflecting the incoming SW energy. Different aerosol types also have different ranges in AOT values. Therefore, the non-linear effect shown in figure 1 is influenced by an averaged effect from all aerosol types.

Where c is the cloud fraction. Equation 1 shows the change in the total (aerosol +cloud) SW flux due to a change in AOT. The aerosol direct effect over clouds is assume to be negligible comparing with the aerosol indirect forcing, and is omitted in equation (1). At the regions with AOT values less than 0.05, a slightly increase in the

number concentration of aerosols (aerosol loading) could effectively nucleate more cloud drops and increase cloud albedo, known as the "Twomey effect" [Ramanathan et al, 2001; Kaufman et al., 2002]. However, due to the low aerosol loading, aerosol direct effect is small, and the first term in the right hand side of the equation 1 is insignificant. Therefore, the aerosol indirect effect dominates. So, based on equation 1, the slope of AOT vs. TOA flux increases as the cloud fraction increases. For AOT range of 0.05 to 0.5, because of the high aerosol loading, the aerosol direct forcing becomes strong as shown in figure 2. Also because clear areas cover more than 80% of a CERES pixel, the aerosol direct forcing term (the first term in the right hand side of the equation 1) dominates at this AOT range and the slope of AOT vs. TOA SW flux decreases as the cloud fraction increases. However, the results shown in figure 3 could be biased by the combination of uncertainties from ADMs, MODIS aerosol retrievals and cloud masking, and need to be examined separately in future studies.

Averaged over all the 0.01 interval AOT bins, the increase in cloudiness from 0% to 0-5%, 5-10%, 10-15% and 15-20% result in increases in the CERES TOA SW fluxes of 4.3, 9.7, 14.5 and 18.2 $Wm^{-2}$ respectively. Therefore, in the clear sky aerosol radiative forcing studies, cloud contamination is one of the largest uncertainties that needs to be carefully examined.

## 4. Discussion and Conclusions

This study shows a new strategy for examining the effect of aerosols on the radiation balance of the earth-atmosphere system through synergistic use of multiple instruments on the same satellite. However, the uncertainties involved in this study should be carefully examined in future studies. One of the largest uncertainties from this approach is the lack of angular dependence models for aerosols. New strategies for developing ADM's for aerosols must be developed as a function of aerosol type and AOT. We address the effect of aerosol ADMs in a companion paper (Zhang and Christopher, same issue). Another major source of uncertainty is associated with deriving $F_{clr}$ and is caused by the uncertainties in MODIS AOT retrievals, uncertainties in surface conditions and lack of clear sky data records in consistent cloud covered areas. Cloud contamination is also a critical issue in the study. The focus of this paper was to examine the global aerosol direct radiative forcing over ocean for cloud free conditions. Averaged over the entire month, the $\tau_{0.55}$ is 0.07 and SWARF is –6 $Wm^{-2}$. This study also showed that dust aerosols are most effective in reflecting the incoming solar energy back to the space than smoke aerosols. Preliminary work on aerosol radiative forcing for all sky conditions also shows that for an observed scene of low cloudiness, the aerosol indirect effect dominates at the low AOT regions, yet at the high AOT regions, the aerosol direct radiative forcing dominates. In this study, SWARF is derived at the Terra overpass time. So the SWARF value derived in this study may not represents the diurnally averaged SWARF. However, this is the first step towards the study of global aerosol radiative forcing using satellite measurements.

## References

Christopher, S. A, J. Chou, J. Zhang, X. Li and R. M. Welch, Shortwave direct radiative forcing of biomass burning aerosols estimated from VIRS and CERES, *Geophys. Res. Lett., 27*, 2197-2200, 2000.

Hansen, J., M. Sato, A. Lacis, R. Ruedy, I. Tegen, and E. Matthews, Climate forcings in the Industrial era, *Proc. Natl. Acad. Sci.*, *95*, 12,753-12,758, 1998.

Haywood, J. M., V. Ramaswamy, and B. J. Soden, Tropospheric aerosol climate forcing in clear-sky satellite observations over the oceans, *Science, 283*, 1299-1303, 1999.

Husar R. B., J. M. Prospero, and L. L. Stowe, Characterization of tropospheric aerosols over the oceans with the NOAA advanced very high-resolution radiometer optical thickness operational product, *J. Geophys. Res.*, *102*, 16889-16909, 1997.

Intergovernmental Panel on Climate Change (IPCC), Climate change 2001, The scientific

basis, *Cambridge University Press*, 881pp, 2001.

Kaufman Y.J., D. Tanré, O. Dubovik, A. Karnieli, and L.A. Remer, Absorption of sunlight by dust as inferred from satellite and ground-based remote sensing, *Geophys. Res. Lett., 28*, 1479-1482, 2001.

Kaufman Y. J., D. Tanré, and O. Boucher, A satellite view of aerosols in the climate system, *Science, 419*, 215-223, 2002.

King, M.D., Y.J. Kaufman, D. Tanré, and T. Nakajima, Remote sensing of tropospheric aerosols from space: Past, Present, and Future, *Bull. Am. Meteorol. Soc.*, *80*, 2229-2259, 1999.

Loeb, N. G., and S. Kato, Top-of-Atmosphere direct radiative effect of aerosols from the Clouds and the Earth's Radiant Energy System Satellite instrument (CERES), *J. Climate, 15*, 1474-1484, 2002.

Olson, J., R., B. A. Baum, D. R. Cahoon, and J. H. Crawford, Frequency and distribution of forest, savanna, and crop fires over tropical regions during PEM-Tropics A, *J. Geophys. Res.*, *104*, 5865-5876, 1999.

Platnick, S., M. D. King, S. A. Ackerman. W. P. Menzel, B. A. Baum, R. A. Frey, The MODIS cloud products: Algorithms and examples from Terra, *IEEE Transactions on Geoscience and Remote Sensing,* sumbmitted, 2002.

Penner, J. E., R. E. Dickinson, and C. A. O'Neill, Effects of aerosol from biomass burning on the global radiation budget, *Science*, *256*, 1432-1434, 1992.

Ramanathan, V., and co-authors, Indian ocean experiment: An intergrated analysis of the climate forcing and effects of the great Indo-Asian haze, *J. Geophys. Res.*, *106*, 28,371-28,398, 2001.

Reid, J. S., P. V. Hobbs, R. J. Ferek, D. R. Blake, J. V. Martins, M. R. Dunlap, and C. Liousse, Physical, chemical and optical properties of regional hazes dominated by smoke in Brazil, *J. Geophys. Res.*, *103*, 32059-32080, 1998.

Remer, L. A., D. Tanré, Y. J. Kaufman, C. Ichoku, S. Mattoo, R. Levy, D. A. Chu, B. N. Holben, O. Dubovik, A. Smirnov, J. V. Martins, R. R. Li, and Z. Ahmad, Validation of MODIS aerosol retrieval over ocean, *Geophys. Res. Lett.*, (2002a, in press).

Remer, L. A., Y. J. Kaufman, Z. Levin and S. Ghan, Model assessment of the ability of MODIS to measure top of atmosphere direct radiative forcing from smoke aerosols. *J. Atmos. Sci.*, 59657-59667, 2002b.

Ross, J. L. ; P. V. Hobbs; B. Holben, Radiative characteristics of regional hazes dominated by

smoke from biomass burning in Brazil: Closure tests and direct radiative forcing, *J. Geophys. Res.,* 103 ,31,925-31,942, 1998.

Tanré, D., Y.J. Kaufman, M. Herman and S. Mattoo, Remote sensing of aerosol properties over oceans using the MODIS/EOS spectral radiances, *J. Geophys. Res.*, *102*, 16971-16988, 1997.

Wielicki, B. A., and R.N. Green, Cloud identification for ERBE radiative flux retrieval, *J. Appl. Meteorol.*, *28*, 1133-1146, 1989.

Wielicki, B. A., B. R. Barkstrom, E. F. Harrison, R. B. Lee III, G. L. Smith, and J. E. Cooper, Clouds and the Earth's Radiant Energy System (CERES): An Earth observing system experiment, *Bull. Am. Meteorol. Soc.*, *77*, 853-868, 1996.

Zhang, J. and S. A. Christopher, Short wave aerosol direct forcing over cloud free oceans from Terra, this issue, 2003.